Magnetic and magneto-elastic properties of a single crystal of TbB_6

2001 J. Phys.: Condens. Matter 13 6307

(http://iopscience.iop.org/0953-8984/13/29/304)

INSTITUTE OF PHYSICS PUBLISHING JOURNAL OF PHYSICS: CONDENSED MATTER

J. Phys.: Condens. Matter **13** (2001) 6307–6321 PII: S0953-8984(01)22020-7

Magnetic and magneto-elastic properties of a single crystal of TbB_6

S A Granovsky[1,3], M Amara[1], R M Galéra[1,4] and S Kunii[2]

[1] Laboratoire Louis Néel[5], CNRS, BP 166, 38042 Grenoble Cédex 9, France
[2] Department of Physics, Faculty of Science, Tohoku University, Aramaki, Aoba-ku, Sendai 980, Japan

Received 15 February 2001
Published 6 July 2001
Online at stacks.iop.org/JPhysCM/13/6307

Abstract

The magnetic and magneto-elastic properties of a single crystal of TbB_6 are studied. In the ordered range metamagnetic behaviours are observed and complex phase diagrams are determined for magnetic fields along fourfold and threefold directions. In the paramagnetic phase the third-order magnetic susceptibilities and the parastriction curves show anisotropic behaviour which could be accounted for by crystalline electric field (CEF) effects. A set of CEF parameters is proposed on the basis of the analysis of the experimental magnetic and quadrupolar susceptibilities. Though non-negligible, the deduced quadrupolar couplings are weak in comparison with those previously determined in PrB_6.

1. Introduction

The rare earth hexaborides, RB_6, crystallize in the CaB_6-type structure, which can be described as a simple CsCl-type arrangement of B_6 octahedra and rare earth ions. The variety of the physical properties observed in these low-carrier-density compounds has been attracting interest for more than two decades. In the domain of applications LaB_6 has received much attention because of its very low work function, which makes it particularly suitable for thermionic emission [1]. In more fundamental research, CeB_6 [2–4] and SmB_6 [5] have been widely studied. SmB_6 is an intermediate-valence compound presenting a semiconductor behaviour at low temperature. CeB_6 is considered as the archetype of the dense Kondo system. CeB_6 is also claimed to present an antiferroquadrupolar ordering in the paramagnetic phase between $T_Q \approx 3.3$ K and $T_N \approx 2.4$ K [6]. However, the mechanisms originating this quadrupolar ordering are still not elucidated. It may be noted that the Kondo coupling on the Ce

[3] Permanent address: Laboratory of Problems on Magnetism, Faculty of Physics, M V Lomonosov Moscow State University, Vorob'evy Gory, 119899 Moscow, Russia.
[4] Author to whom correspondence should be addressed.
[5] Laboratory associated with the Université Joseph Fourier de Grenoble, France.

0953-8984/01/296307+15$30.00

ions makes difficult a clear analysis of these mechanisms within the usual formalism. In PrB_6, which shows properties reminiscent of CeB_6, Morin *et al* [7] have confirmed that negative quadrupolar pair interactions exist in the paramagnetic phase ($T_N = 6.9$ K). Nevertheless they pointed out that additional couplings have to be considered to completely understand the behaviour of PrB_6. The properties of GdB_6 appear also very unusual. For instance its Néel temperature, $T_N = 15$ K, is anomalously small compared with the other heavy rare earth compounds. Fisk *et al* [8] have suggested that short range order sets in the paramagnetic phase. Unexpectedly for an S-state system, GdB_6 exhibits a first-order type transition at T_N and, in addition, a second magnetic transition occurs at $T^* = 8.6$ K [9, 10]. Up to now the magnetic structures and their microscopic origins remain unknown. By reason of their incongruent melting, which makes the growth of single crystals difficult [11], the other heavy rare earth hexaborides have been less investigated [12–14]. TbB_6, DyB_6 and HoB_6 have been reported to order antiferromagnetically at $T_N = 19.5$, 25.6 and 5.6 K respectively [12]. The important softening of the elastic constant C_{44} observed in these three compounds suggests that noticeable magneto-elastic couplings and, possibly, quadrupolar pair interactions are active in these compounds [13].

It is now well established that among the different types of interaction present in the rare earth ion (R) based systems, the quadrupolar ones deeply influence the magnetic and magneto-elastic properties [15]. They can affect the order and the temperature of the magnetic transitions, stabilize an easy magnetization direction different from that determined by the crystalline electric field (CEF) and also contribute to the selection of the magnetic structure. For instance negative quadrupolar (antiferroquadrupolar) interactions stabilize multi-axial spin arrangements. This is well illustrated by intermetallic compounds of the CsCl-type family like TmCu, DyAg or NdZn [16–20]. The interplay between quadrupolar, CEF, bilinear and magneto-elastic interactions gives rise to complex (H, T) magnetic phase diagrams. In some cases the quadrupolar pair interactions can be large enough to dominate the bilinear ones, leading to a pure quadrupolar ordering in the paramagnetic phase. The occurrence of ferroquadrupolar orderings in TmZn, TmCd or CeAg [21] is unambiguously supported by the consistency of the analysis of the numerous experimental results. The existence of purely antiferroquadrupolar phases, as proposed for $PrPb_3$ [22], $TmGa_3$ [23] or CeB_6, is less clear.

The understanding of the specific properties of CeB_6 will strongly benefit from a complete insight into the properties in the rest of the RB_6 series. We have undertaken the study of TbB_6 with the aim of determining interplay and strength of the different type of interaction in this compound. Here we first present the magnetic and magneto-elastic measurements performed on a single crystal in the ordered and paramagnetic phases. In a second part, we develop an analysis of the experimental results in the paramagnetic phase within the CEF susceptibility formalism.

2. Experimental conditions

The single crystals of TbB_6 are grown by the crucible-free vertical floating zone technique under pressurized high-purity argon gas [11]. In the present work we used the same single crystal, a sphere of 3.1 mm diameter, for magnetization and magnetostriction measurements. Both type of measurement were performed at the Laboratoire Louis Néel.

The magnetization processes were measured by the extraction method in the temperature range 1.5–300 K. Two cryomagnets which supply magnetic fields up to 11 and 16 T respectively were used. The sensitivity of the measurements reaches 5×10^{-4} emu in the whole temperature range. Isofield and isothermal magnetization curves were measured with the magnetic fields

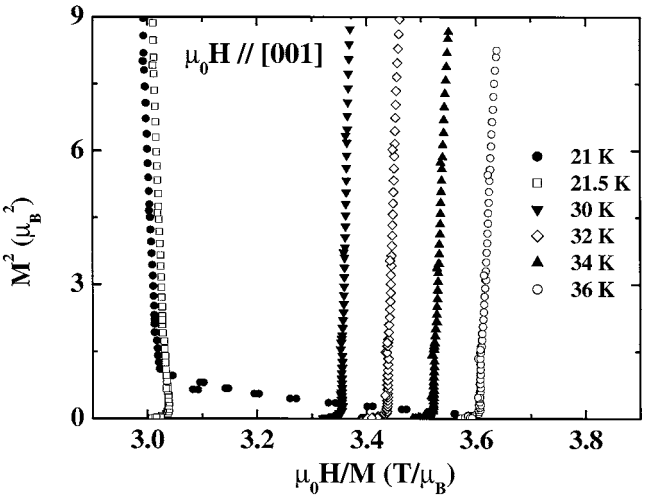

Figure 1. Arrotts plots deduced from the magnetization curves measured with the magnetic field applied along a fourfold axis. The change of the initial slope of the curve at 21 K indicates that the ordered phase is reached.

applied successively along the fourfold and threefold axes of the cubic crystallographic structure.

The magnetostriction measurements were performed using a high-accuracy capacitance dilatometer. The set-up allows measurements of the thermal expansion and the magnetostriction in the temperature range 3–250 K, under magnetic fields up to 6.5 T with a typical resolution less than 1 Å. Thanks to the rotation of the capacitance cell around the vertical axis of the cryostat it is possible to adjust the angle between the probed axis and the horizontal field direction. When the measurements are performed along the fourfold axis for instance, both the parallel, $\Delta l_{\parallel}$, and the perpendicular, $\Delta l_{\perp}$, changes of length can be measured within a single run.

3. The paramagnetic phase

3.1. Magnetization measurements

The first-order magnetic susceptibility, $\chi^{(1)}$, of TbB_6 was deduced from the Arrotts plots: $M^2 = f(H/M)$. As shown in figure 1, the plots have a linear behaviour at all temperatures in the range 21.5–300 K. Below 21.5 K, the curves change slope in the low-field region, indicating that the ordered phase was reached. It can then be determined that T_N ranges between 21 and 21.5 K. The thermal variation of the inverse of the first-order susceptibility in fields applied along the fourfold and threefold directions respectively is reported in figure 2. Both thermal variations follow a Curie–Weiss law and, as expected for a cubic compound, no anisotropy is observed. The effective magnetic moment deduced from the experimental slope is $\mu_{eff} = 9.65 \pm 0.02\ \mu_B$, in good agreement with the theoretical value for the Tb^{3+} ion, $\mu_{eff} = 9.721\ \mu_B$. The intercept of the Curie–Weiss line with the temperature axis yields a paramagnetic Curie temperature, θ_p, of -38.7 ± 1 K.

The third-order magnetic susceptibility, $\chi^{(3)}$, was deduced in the paramagnetic domain from the slope of the Arrotts plots: $\chi^{(3)} = -[\chi^{(1)}]^4[\Delta(\mu_0 H/M)/\Delta M^2]$. Figure 3 shows the thermal variation of the third-order susceptibility determined for both the tetragonal ($H \parallel [001]$

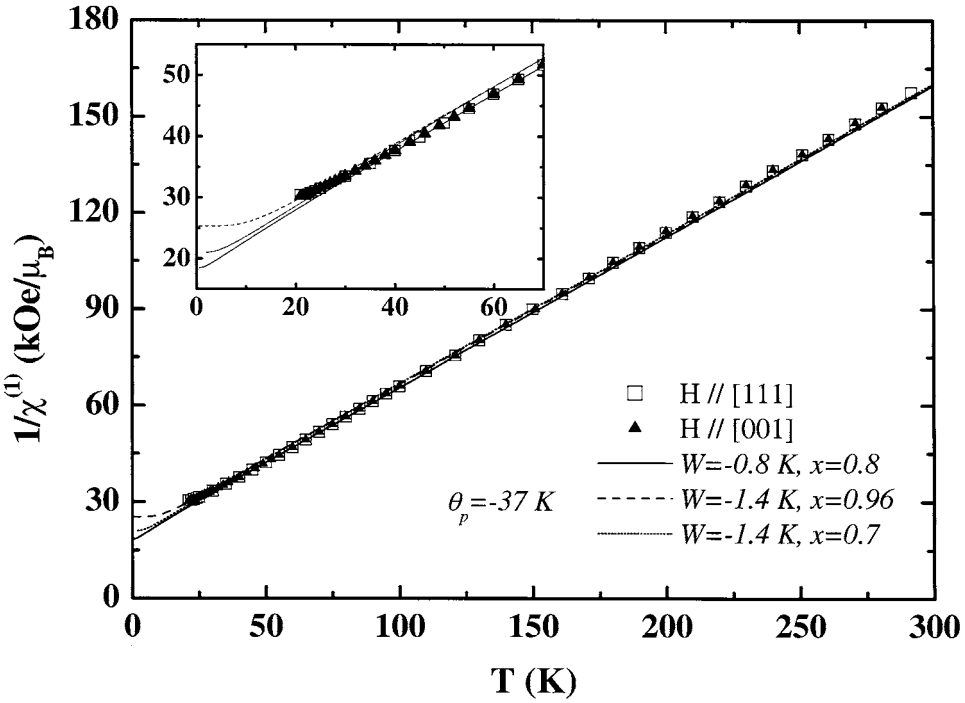

Figure 2. Thermal variation of the inverse of the first-order susceptibility, $1/\chi^{(1)}$, determined for magnetic fields applied along the [111] (open squares) and [001] (full triangles) axes. The lines represent the thermal variation of $1/\chi^{(1)}$ calculated with the sets of CEF parameters given in the figure and $\theta_p = -37$ K.

axis) and the trigonal ($H \parallel$ [111] axis) symmetries. The experimental curves exhibit a large anisotropy in a wide range of temperatures, up to 150 K. In the tetragonal symmetry $\chi^{(3)}$ is negative at high temperature. While cooling, it first decreases, passes through a shallow minimum around 40 K, then starts to sharply increase and becomes positive below 25 K. In the trigonal symmetry $\chi^{(3)}$ remains negative in the whole studied temperature range. However, it presents a much steeper decrease than in the tetragonal symmetry when cooling and a well peaked minimum is observed at 30 K.

3.2. Parastriction measurements

In the paramagnetic phase the field-induced relative change of lengths, $(\Delta l/l)_\parallel = \lambda_\parallel$, along the field direction, and $(\Delta l/l)_\perp = \lambda_\perp$ perpendicular to it, were measured in fields up to 5 T, applied successively along the [001] and [111] axes. Figure 4 shows the variation of the tetragonal symmetry strain, $\lambda_\parallel - \lambda_\perp$, as a function of the square of the field. In fields larger than 1.5 T, $\lambda_\parallel - \lambda_\perp$ varies linearly with H^2. The same dependence is observed for the trigonal strain. $\lambda_\parallel - \lambda_\perp$ is found to be negative for both the tetragonal and trigonal modes. The thermal variation of $H/\sqrt{|\lambda_\parallel - \lambda_\perp|}$ has been deduced for the trigonal mode ($H \parallel$ [111]) with a good accuracy up to 250 K (figure 5(a)). Above 50 K, $H/\sqrt{|\lambda_\parallel - \lambda_\perp|}$ increases linearly with the temperature, according to a Curie-like law. Below this temperature its behaviour is much more of Van Vleck type. The determination of $H/\sqrt{|\lambda_\parallel - \lambda_\perp|}$ in the tetragonal mode ($H \parallel$ [001]) is less precise due to the weaker magneto-elastic couplings in this mode as observed by Nakamura *et al* in sound velocity measurements [13]. In this last mode, $H/\sqrt{|\lambda_\parallel - \lambda_\perp|}$ increases linearly

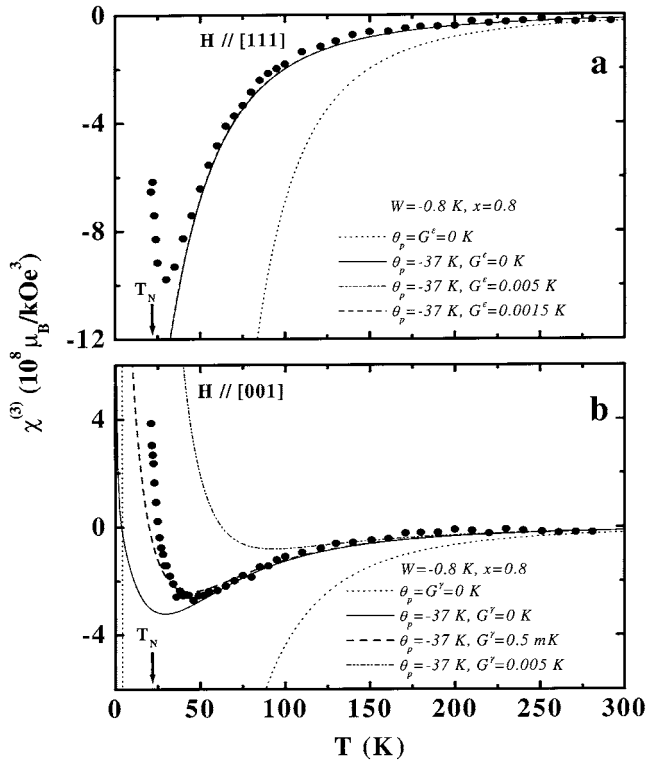

Figure 3. Thermal variation of the third-order magnetic susceptibility, $\chi^{(3)}$, determined (a) for fields applied along a threefold axis (trigonal symmetry), (b) for fields applied along a fourfold axis (tetragonal symmetry). The lines represent the calculated third-order susceptibilities using the set $W = -0.8$ K, $x = 0.8$, for the CEF parameters and the values of the dipolar, θ_p, and quadrupolar, $G^{\varepsilon,\gamma}$, constants indicated in the figure. Note that in the trigonal symmetry, the curves calculated with different values of the quadrupolar constants are all superimposed.

with the temperature in the whole studied range (figure 5(b)). Therefore, like the third-order magnetic susceptibility, the parastriction presents an anisotropic behaviour.

4. Magnetization processes in the ordered phase

In the ordered range isothermal and isofield magnetization curves were collected for fields applied along the fourfold and threefold axes. Along both axes the magnetization processes of the sphere reveal metamagnetic transitions.

At 2 K, for a field along the [001] axis, two transitions are observed at $\mu_0 H_{c1} = 9$ T and $\mu_0 H_{c2} = 12.2$ T on the magnetization curve. At each jump the magnetization is increased by about 1 μ_B. A third jump occurs at $\mu_0 H_{c3} = 14$ T. Under an applied field of 14.5 T, the magnetization reaches 5.25 μ_B. This value is far from the 9 μ_B expected for the saturated moment of the Tb^{3+} ion. This indicates that the field polarized paramagnetic state is still not reached. Decreasing the field a large hysteresis is observed for all the transitions as shown in figure 6(a). Figure 6(a) also compares the magnetization at 2 and 3 K. At 3 K the magnetization shows again steep steps at 9 and 12.2 T. The jump at 14 T is strongly damped and shows no hysteresis. Increasing the temperature the structures in the magnetization curves

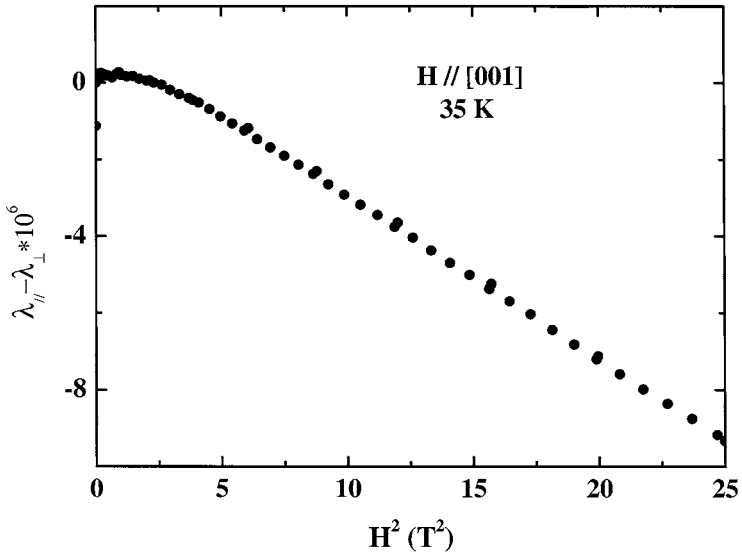

Figure 4. Evolution of the tetragonal symmetry strain, $\lambda_{\parallel} - \lambda_{\perp}$, as a function of the applied magnetic field at $T = 35$ K.

progressively smooth off and the hysteresis decreases. The critical fields were then deduced from the derivatives $\mathrm{d}M/\mathrm{d}H$ as shown in figure 6(b). The isofield measurements have allowed to determine the evolution of the paramagnetic-ordered phase transition line as function of the field. The maximum of the $M(T)$ curves defines the transition temperature. Below this temperature and for some values of the applied field, the $M(T)$ curves show changes in the slope (see figure 7), which generally evidence phase transitions. The different features observed in both the isothermal and the isofield processes allowed one to build the (H, T) magnetic phase diagram when the field is along the fourfold axis. This diagram is presented in figure 8(a). Extrapolating down to zero field the paramagnetic-ordered phase transition line leads to a Néel temperature of 21 K in agreement with the determination from the Arrotts plots. T_N is then slightly larger than the value previously reported [12]. In the ordered range the three phases, I, II and III are unambiguously established by jumps in the magnetization curve itself. The lines between phases II and II′ or III and III′ were deduced from maxima in the derivatives (see figure 6(b)). Structures in the isofield curves apparently confirm the line between phases II and II′. But, as expected for horizontal transition lines, no anomalies associated with the phase III–phase III′ transition are observed in the isofield curves. The existence of phase III′ is then more questionable.

For fields applied along a threefold axis the magnetization process at 1.77 K presents four steps at 9.7, 11.1, 11.9 and 12.4 T respectively (see figure 9). Decreasing the field a hysteresis is again observed at these transitions, but much weaker than along the [001] axis. Under the maximum value of the applied field, 14.5 T, the magnetization reaches only 5.2 μ_B. In this case also the field-polarized paramagnetic phase is far for being reached. The evolution of the magnetization curves as function of the temperature is illustrated in figure 9. The two highest transitions rapidly merge together and above 4 K only one transition remains. Further increasing the temperature the low-field transition also smooths off and above 6 K it has completely disappeared. Figure 10 shows the thermal evolution of the magnetization under several applied fields. The (H, T) magnetic phase diagram built for fields along the [111] axis

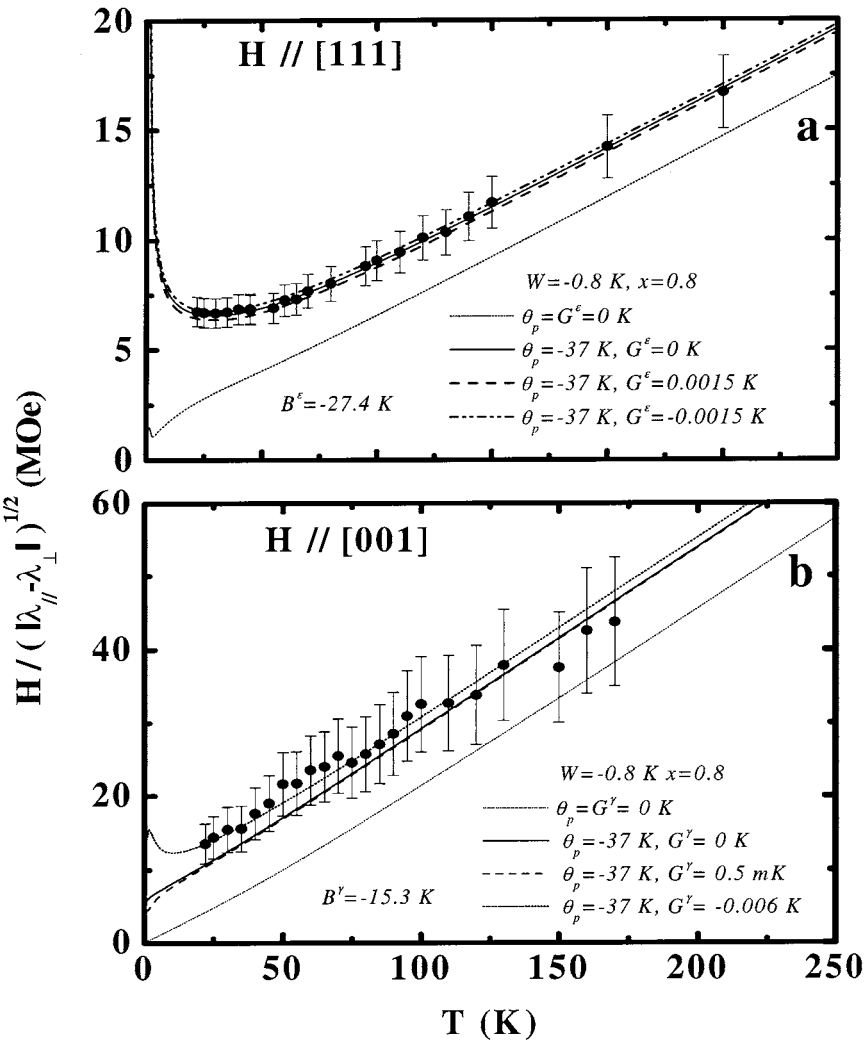

Figure 5. Full dots represent the experimental thermal variation of $H/\sqrt{|\lambda_{\parallel} - \lambda_{\perp}|}$, (a) in the trigonal mode ($H \parallel [111]$), (b) in the tetragonal mode ($H \parallel [001]$). The lines represent the calculations performed with $W = -0.8$ K, $x = 0.8$ and the magneto-elastic coefficients $B^{\varepsilon} = -27.4$ K and $B^{\gamma} = -15.3$ K, using the values of the dipolar, θ_p, and quadrupolar, $G^{\varepsilon,\gamma}$, constants given in the figure.

is presented in figure 8(b). One remarkable feature is the existence of a critical point ending the line between phases I and I′. A very similar feature has been observed in the phase diagram of the ternary compound DyAlGa by Gignoux *et al* [24]. Phase II becomes very narrow above 7 K but seems to extend up to 15 K. The evolution as a function of the field of the transition temperature, between ordered and paramagnetic phases, is very similar to the one observed along the [001] axis (figure 8(a)).

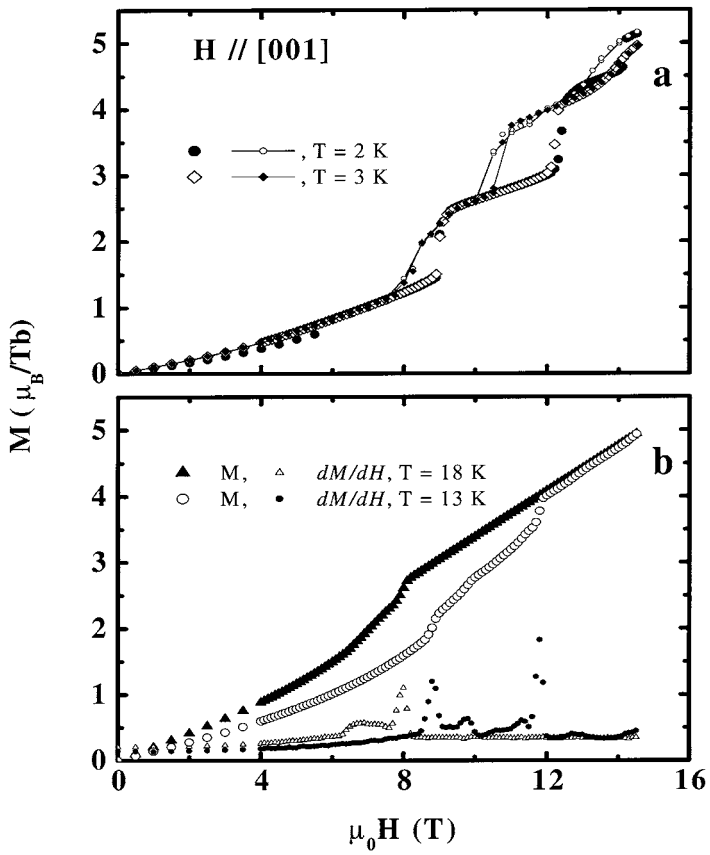

Figure 6. Field applied along a fourfold axis. (a) Magnetization curves measured at 2 K (full and open dots) and 3 K (open and full diamonds). Line symbols represent the measurements decreasing the magnetic field. (b) Magnetization curves measured at 13 K (open dots) and 18 K (full triangles). The full dots and open triangles represent the derivatives, $\mathrm{d}M/\mathrm{d}H$, at $T = 13$ and 18 K respectively.

5. Analysis within the CEF-susceptibility formalism

The measurements of elastic constants, parastriction and third-order magnetic susceptibilities are valuable methods to study the quadrupolar interactions in rare earth compounds. Starting from the knowledge of the CEF parameters, the CEF-susceptibility formalism developed by Morin and Schmitt [15] has allowed, for many rare earth systems, a quantitative analysis of the quadrupolar interactions in the paramagnetic phase. Conversely the susceptibility formalism may be in some cases an alternative method to determine these CEF parameters. For instance in $TbIn_3$, the CEF scheme was successfully determined by fitting the different susceptibilities measured on a dilute compound [25]. The basic Hamiltonian used to describe, in a quantum approach, the magnetic and magneto-elastic properties of the rare earth ions is the sum of the CEF Hamiltonian, $\mathcal{H}_{CEF}$, the exchange interactions and the Zeeman coupling, $\mathcal{H}_J$, the magneto-elastic, $\mathcal{H}_{ME}$, and the quadrupolar, $\mathcal{H}_Q$, Hamiltonians. The spin Heisenberg-type exchange, the quadrupolar and the magneto-elastic couplings are treated within the mean field approximation (MFA). The expressions of all these Hamiltonians are given in [15]. Generally in the paramagnetic phase the one-ion CEF Hamiltonian is first diagonalized and the remaining

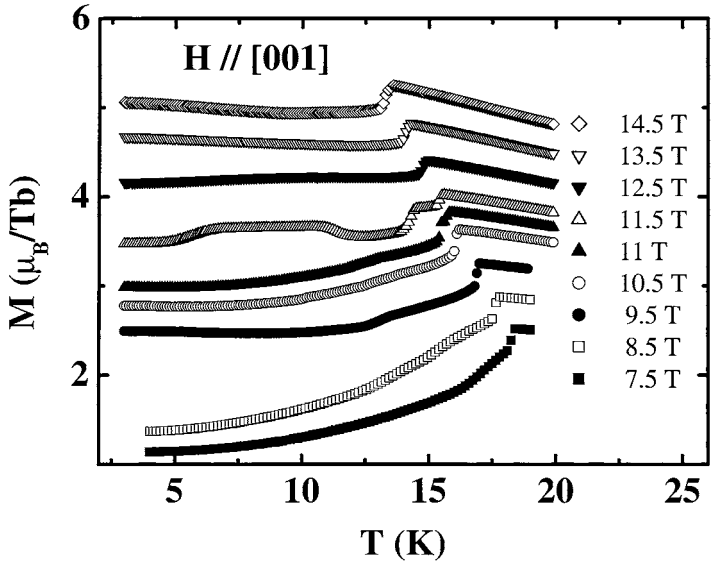

Figure 7. Thermal evolution of the magnetization measured for several values of the field applied along the fourfold axis.

terms, $\mathcal{H}_1 = \mathcal{H}_J + \mathcal{H}_{ME} + \mathcal{H}_Q$, are treated applying the perturbation method. The expansion is carried out up to the second order for the strain components, $\varepsilon^{\mu=\gamma,\varepsilon}$, the quadrupolar operators, $Q = \langle O_2^0 \rangle$ or $P = \langle P_{ij} \rangle$, and to the fourth order for the field, H, and the magnetic moment M. As in a cubic symmetry, the two normal strain modes can be fully decoupled according to the external stress direction, the tetragonal (γ) and the trigonal (ε) modes can be considered separately. From the partition function an analytical expression for the free energy is derived, which includes the four CEF single-ion susceptibilities: χ_0, $\chi_{\mu=\gamma,\varepsilon}$, $\chi^{(2)}_{\mu=\gamma,\varepsilon}$ and $\chi^{(3)}_{\mu=\gamma,\varepsilon}$. χ_0 is the usual first-order magnetic susceptibility. $\chi_{\mu=\gamma,\varepsilon}$ is a quadrupolar strain susceptibility and $\chi^{(2)}_{\mu=\gamma,\varepsilon}$ a quadrupolar field susceptibility, which couples the quadrupolar operator to the magnetic field. Finally $\chi^{(3)}_{\mu=\gamma,\varepsilon}$ is the third-order magnetic susceptibility related to the initial curvature of the magnetization processes. All these susceptibilities depend only on the cubic CEF scheme and on the matrix elements of the magnetic dipolar (J) and electric quadrupolar (O_2^0, P_{ij}) operators between the CEF eigenfunctions (appendices 3 and 4 in [15]). The equilibrium values of M, Q or P and ε are deduced from the minimization of the free energy. In the tetragonal mode γ, this leads to the following coupled expressions:

$$M = g_J \mu_B \langle J_z \rangle = \chi_M H + \chi_M^{(3)} H^3 \qquad \text{with}$$

$$\chi_M = \frac{\chi_0}{1 - n\chi_0} \qquad \text{and} \qquad \chi_M^{(3)} = \frac{1}{(1 - n\chi_0)^4} \left[\chi_\gamma^{(3)} + 2G^\gamma \frac{(\chi_\gamma^{(2)})^2}{1 - G^\gamma \chi_\gamma} \right]$$

$$\varepsilon_1^\gamma = \frac{B^\gamma}{C_0^\gamma} \langle O_2^0 \rangle = \frac{B^\gamma}{C_0^\gamma} Q \qquad \text{and} \qquad Q = \chi_Q H^2 \qquad \text{with}$$

$$\chi_Q = \frac{\chi_\gamma^{(2)}}{(1 - n\chi_0)^2 (1 - G^\gamma \chi_\gamma)}. \tag{1}$$

In these expressions, n and G^γ are the bilinear exchange and the total quadrupolar constants respectively. G^γ is defined as $G^\gamma = [(B^\gamma)^2 / C_0^\gamma] + K^\gamma$. B^γ is the magneto-elastic coupling constant, $C_0^\gamma = C_{11}^0 - C_{12}^0$ the background elastic constant and K^γ the two-ion quadrupolar

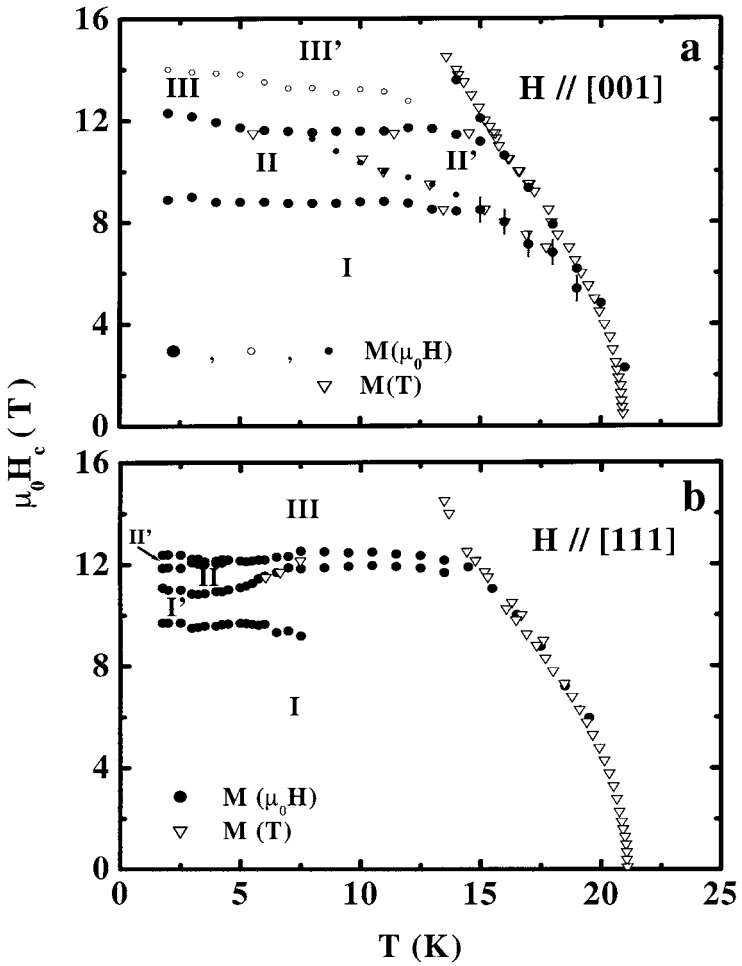

Figure 8. (a) (H, T) magnetic phase diagram for magnetic fields applied along a fourfold axis. The large full dots represent the steps directly observed on the isothermal magnetic processes. The small full and open dots represent the structures obtained from the derivatives $\mathrm{d}M/\mathrm{d}H$. The open triangles correspond to the features observed on the isofield curves. (b) (H, T) magnetic phase diagram determined for fields along a threefold axis. The full dots represent the steps observed in the isothermal magnetization curves and the open triangles the structures in the $M(T)$ curves.

coupling constant. In the limit of $H = 0$, the equilibrium conditions allow us to deduce the following relation for the elastic constant:

$$C^{\gamma} = C_0^{\gamma} - \frac{(B^{\gamma})^2 \chi_{\gamma}}{(1 - K^{\gamma}\chi_{\gamma})}. \tag{2}$$

For the trigonal mode the non-zero terms are $M = \sqrt{3} g_J \mu_B \langle J_z \rangle$ with $\langle J_z \rangle = \langle J_x \rangle = \langle J_y \rangle$, $P = \langle P_{xy} \rangle = \langle P_{yz} \rangle = \langle P_{zx} \rangle$ and $\varepsilon^{\varepsilon} = \varepsilon_1^{\varepsilon} = \varepsilon_2^{\varepsilon} = \varepsilon_3^{\varepsilon}$. The minimization of the free energy leads then to the expressions:

$$M = \chi_M H + \chi_M^{(3)} H^3 \qquad \text{with} \qquad \chi_M^{(3)} = \frac{1}{(1 - n\chi_0)^4} \left[\chi_{\varepsilon}^{(3)} + 6G^{\varepsilon} \frac{(\chi_{\varepsilon}^{(2)})^2}{1 - G^{\varepsilon}\chi_{\varepsilon}} \right]$$

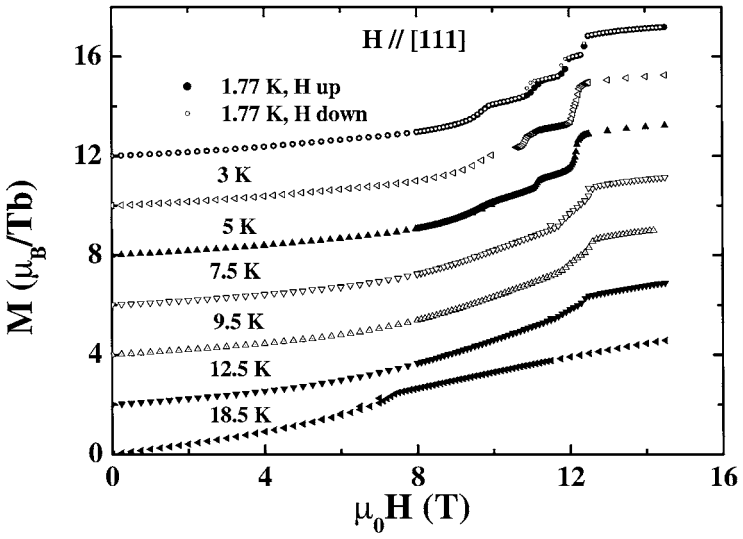

Figure 9. Isothermal magnetization processes at different temperatures for fields applied along a threefold axis. At $T = 1.77$ K, full dots represent the measurements increasing the field and open dots measurements decreasing the field. For clarity the curves have been offset by 2 μ_B.

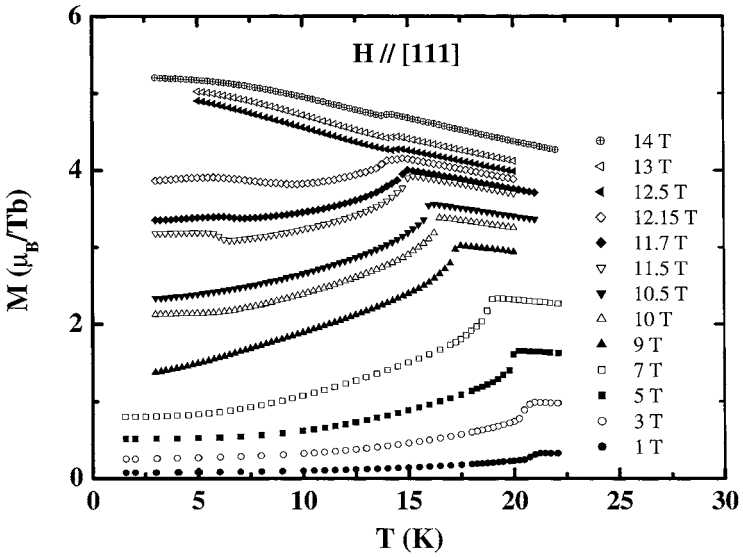

Figure 10. Isofield magnetization curves for fields applied along the [111] axis.

$$\varepsilon^{\varepsilon} = \frac{B^{\varepsilon}}{C_0^{\varepsilon}} P \qquad \text{and} \qquad P = \chi_P H^2 \qquad \text{with} \qquad \chi_P = \frac{\chi_{\varepsilon}^{(2)}}{(1 - n\chi_0)^2 (1 - 3G^{\varepsilon}\chi_{\varepsilon})} \tag{3}$$

$$C^{\varepsilon} = C_0^{\varepsilon} - \frac{3(B^{\varepsilon})^2 \chi_{\varepsilon}}{(1 - 3K^{\varepsilon}\chi_{\varepsilon})}. \tag{4}$$

It is therefore possible to determine unambiguously the values of all the coupling parameters by fitting the thermal variation of the different experimental susceptibilities,

provided the CEF scheme is known in another way. The first- (χ_M) and third-order ($\chi_M^{(3)}$) magnetic susceptibilities are directly deduced from the magnetization measurements when the field is applied along the [001] axis, mode γ, or along [111], mode ε. The quadrupolar susceptibilities ($\chi_{Q,P}$) can be obtained from elastic constant and parastriction measurements. Indeed in the paramagnetic phase the relative macroscopic change in length λ induced by an applied magnetic field is related to the quadrupolar susceptibilities by the following expressions:

$$(\lambda_\parallel - \lambda_\perp)_\gamma = \sqrt{\frac{3}{2}}\frac{B^\gamma}{C_0^\gamma}\chi_Q H^2 \qquad \text{and} \qquad (\lambda_\parallel - \lambda_\perp)_\varepsilon = \frac{3}{\sqrt{2}}\frac{B^\varepsilon}{C_0^\varepsilon}\chi_P H^2. \tag{5}$$

$\lambda_\parallel$ and $\lambda_\perp$ are the relative change in length measured successively parallel and perpendicular to the direction of the applied field. Both expressions are often written in a linearized way:

$$\frac{H}{\sqrt{|\lambda_\parallel - \lambda_\perp|_\gamma}} = \left(\frac{2}{3}\right)^{1/4}\left(\frac{C_0^\gamma}{B^\gamma}\right)^{1/2}\chi_Q^{-1/2} \qquad \text{and}$$

$$\frac{H}{\sqrt{|\lambda_\parallel - \lambda_\perp|_\varepsilon}} = \left(\frac{\sqrt{2}}{3}\right)^{1/2}\left(\frac{C_0^\varepsilon}{B^\varepsilon}\right)^{1/2}\chi_P^{-1/2}. \tag{6}$$

In the whole RB_6 series the thermal variation of the tetragonal $(C_{11} - C_{12})/2$ elastic constant presents no remarkable anomaly while strong magneto-elastic coupling effects are observed for the trigonal C_{44} elastic constant. TbB_6 [13] shows the weakest softening of the C_{44} mode: only 7%, compared to 70% in DyB_6 and HoB_6 or 34% in PrB_6. This lets us assume weaker quadrupolar interactions in TbB_6. So far the CEF schemes of the heavy rare earth hexaborides are still unknown preventing any quantitative determination of these couplings. Present results on TbB_6 reveal an important anisotropy of the third-order magnetic susceptibility in a wide range of temperatures. Such an anisotropy could be accounted for by CEF effects. Very large CEF level spacings have been reported for the light rare earth hexaborides [26, 27], associated with large negative fourth-order terms ($A_4\langle r^4\rangle \approx -200$ K) and small positive sixth-order terms ($A_6\langle r^6\rangle \approx +6$ K). As generally observed in rare earth compounds, it is likely that within the RB_6 series the CEF parameters keep their signs and that the relative weight between the fourth- and sixth-order parameters does not change drastically. According to the diagrams of Lea *et al* [28] $A_4\langle r^4\rangle < 0$ and $A_6\langle r^6\rangle > 0$ yield either the Γ_2 singlet or the Γ_3 doublet as CEF ground state for the Tb^{3+} ions. Moreover the weak amplitude of the sixth-order term with respect to the fourth-order one would lead to values of x ranging from 0.5 to 1. Assuming that, different sets of CEF parameters have been tested in order to describe simultaneously the first- and third-order magnetic susceptibilities, the parastriction and the elastic constants with a consistent set of bilinear exchange, quadrupolar ($G^{\gamma,\varepsilon}$, $K^{\gamma,\varepsilon}$) and magneto-elastic ($B^{\gamma,\varepsilon}$) parameters. As shown in figure 2 the first-order susceptibility is not very selective for the CEF parameters, but allows one to adjust the value of the paramagnetic Curie temperature θ_p to -37 K. This value was then kept constant in the calculations of the third-order susceptibilities and the parastriction curves. The attempts to reproduce the thermal evolution of the parastriction in the trigonal symmetry (equation (6)) definitively rule out a Γ_3 ground state. Therefore the parameter x must be larger than 0.82. Among the tested sets of CEF parameters the one which best describes the thermal variation of the various susceptibilities is $W = -0.8$ K, $x = 0.8$ (or $A_4\langle r^4\rangle = -87$ K, $A_6\langle r^6\rangle = 19$ K). This corresponds to a singlet Γ_2 ground state with the $\Gamma_5^{(2)}$ and Γ_3 excited levels respectively at 3.5 and 5.1 K. The other excited levels, $\Gamma_5^{(1)}$, Γ_4 and Γ_1 range successively at 118.1, 130.6 and 148.5 K above the ground state. The calculations with this set of parameters are reported in figures 3 and 4 and compared with the experimental data. The third-order susceptibility is very sensitive to the

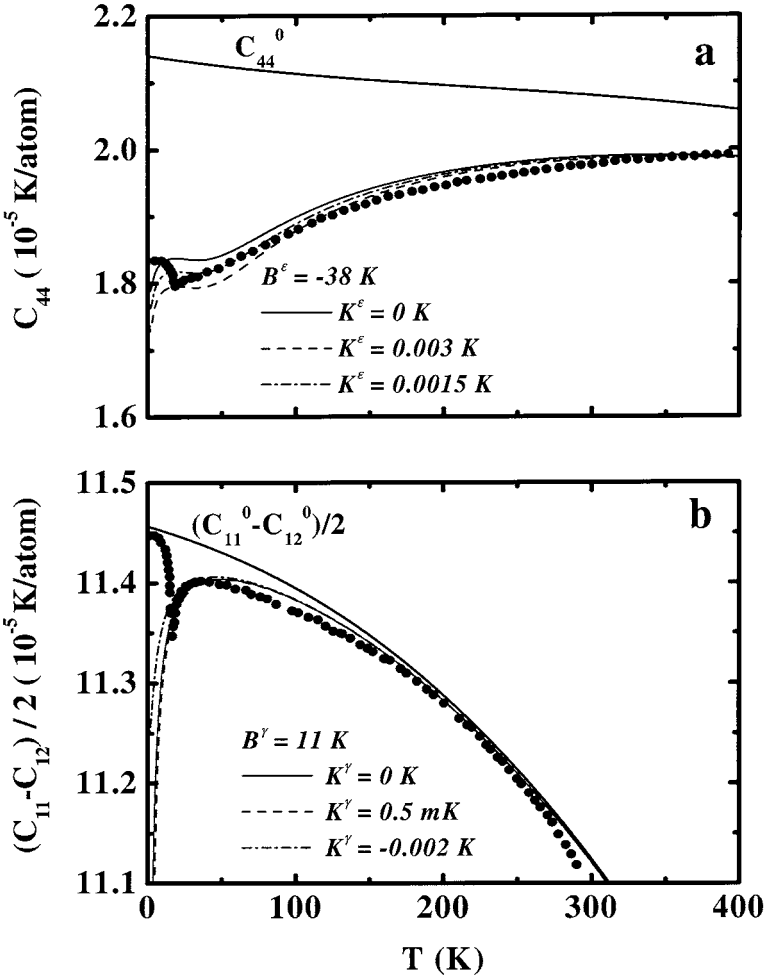

Figure 11. Thermal dependence of the elastic constants in TbB_6 for the trigonal (a) and tetragonal (b) symmetry lowering modes (data from [13]). The background elastic constants, C_{44}^0 and $(C_{11}^0–C_{12}^0)/2$, are deduced from the data in GdB_6 [13]. The lines represent the thermal variation of the elastic constants calculated with the CEF set parameters, $W = -0.8$ K, $x = 0.8$, and using the values of $B^{\gamma,\varepsilon}$ and $K^{\gamma,\varepsilon}$ given in the figure.

paramagnetic Curie temperature, thus confirming the value of -37 K for θ_p. It turns out that the quadrupolar coefficient strongly affects the behaviour of $\chi_M^{(3)}$ in the tetragonal mode below 100 K; the best agreement is obtained for $G^\gamma = 0.5$ mK. In contrast, in the trigonal mode, the correction due to the quadrupolar interactions has negligible effects compared to that due to the exchange interactions. Calculations with quadrupolar coefficients ranging from -0.8 to +0.8 K cannot be distinguished from the curve calculated with $G^\varepsilon = 0$ K and $\theta_p = -37$ K. For clarity in figure 3(a), only the calculations with $G^\varepsilon = 0$, 0.005 and 0.0015 K are presented.

In the calculations of the parastriction, the ratios $C_0^{\gamma,\varepsilon}/B^{\gamma,\varepsilon}$ were deduced from the slope at high temperature of $H/\sqrt{|\lambda_\parallel - \lambda_\perp|_{\gamma,\varepsilon}}$, which has a Curie-like variation (line $\theta_p = G^{\gamma,\varepsilon} = 0$ K in figure 5). The thermal evolution of the TbB_6 background elastic constants was adjusted from the evolution reported in [13] for the GdB_6 constants (see figure 11). The extrapolation

at $T = 0$ K of these curves leads to $(C^0_{11} - C^0_{12})/2 = 11.45 \times 10^{-5}$ K/atom and $C^0_{44} = 2.1 \times 10^{-5}$ K/atom in TbB_6. Using these values, the following magneto-elastic coefficients were obtained: $B^\gamma = -15 \pm 2$ K/atom and $B^\varepsilon = -27 \pm 2$ K/atom. As shown in figure 5 the variation of the parastriction is mainly accounted for by the bilinear exchange and the CEF interactions. The existence of quadrupolar interactions cannot be ruled out, but, within the experimental accuracy it is not possible to determine their sign; indeed G^ε may range from -0.005 to $+0.005$ K, and G^γ from -0.006 to 5×10^{-4} K.

We also calculated the thermal evolution of the elastic constants measured by Nakamura *et al* [13]. In figure 11 are presented the thermal variations of the C_{44} and $(C_{11} - C_{12})/2$ elastic constants calculated with $W = -0.8$ K and $x = 0.8$. The calculations reproduce with a good agreement the experimental data in both the trigonal and the tetragonal symmetry lowering modes using $|B^\varepsilon| = 38$ K and $|B^\gamma| = 11$ K. Though $|B^\varepsilon|$ is slightly larger, these values are consistent with those used to fit the parastriction curves. When normalized by the second-order Stevens coefficient, the values of the magneto-elastic coefficients, $B^\varepsilon/\alpha_J = 3762$ or 2673 K/atom and $B^\gamma/\alpha_J = 1089$ or 1485 K/atom, compare well with those found in other intermetallics [15, 25] but are much smaller than the value of 25 000 K/atom found for B^ε/α_J in PrB_6. Note that, like in the case of the parastriction or the third-order susceptibility, the quadrupolar couplings apparently do not play the main role in the thermal evolution of the elastic constants. Nevertheless the best adjustments lead to values of $K^\varepsilon = 0.0015$ K and $K^\gamma = 0.5$ mK consistent with the values of the total quadrupolar coefficients $G^{\gamma,\varepsilon}$ previously determined.

6. Conclusion

In the paramagnetic phase of TbB_6, the analysis of the magnetic and magneto-elastic susceptibilities within the CEF susceptibilities formalism, has been worked out using a coherent set of parameters. The values of the CEF parameters thus determined for TbB_6 are in fairly good agreement with those reported in the light rare earth hexaborides [26, 27]. Within this CEF scheme the anisotropic behaviour of the third-order magnetic susceptibility is well reproduced. The calculations show that the magnetic pair interactions (θ_p) are the main factor to describe the magnetic and magneto-elastic properties of TbB_6. The intensity of the quadrupolar couplings is found to be very weak compared to those determined in PrB_6 [7]. Indeed the quadrupolar parameters, $G^{\varepsilon,\gamma}$, in TbB_6 are of the order of 1.5–0.5 mK while in PrB_6 they reach values hundred times larger. These weak quadrupolar couplings are therefore in agreement with the weak softening of the elastic constants [13].

In the ordered range the magnetization measurements on this single crystal have revealed several field-induced phases. The magnetic phase diagrams deduced for the first time in this compound appear very complex with, for instance, up to three different phases in the tetragonal symmetry. It is likely that the occurrence of field-induced phases is the signature of multi-q spin arrangements. The possibility of a triple-q magnetic structure in zero field has been previously reported for DyB_6 where a multi-step metamagnetic behaviour of the magnetization has also been observed at 4.2 K [29]. To characterize the actual nature of the magnetic phases it is necessary to perform neutron diffraction studies on a single crystal. This requires the preparation of a new single crystal with ^{11}B enriched boron. In absence of such a sample, x-ray scattering could be an alternative way of determining the magnetic structures. In GdB_6 for instance x-ray diffraction experiments have revealed changes in the charge periodicity associated with the two antiferromagnetic phases. In the case of TbB_6 a possible occurrence of new periodicities in the charge diffraction spectrum could be driven by 4f asphericity effects, as the orbital moment is not null for Tb^{3+} ions. In rare earth compounds

the 4f asphericity should develop according to the symmetries of the ordered magnetic phases. Therefore multipolar x-ray scattering experiments may give access to the actual magnetic structures.

References

[1] Shimizu R, Shinike T, Ichimura S, Kawai S and Tanaka T 1978 *J. Vac. Sci. Technol.* **15** 922
[2] Winzer K and Flesch W 1978 *J. Physique Coll.* **39** C6 832
[3] Takase A, Kojima K, Komatsubara T and Kasuya T 1980 *Solid State Commun.* **36** 461
[4] Sato N, Kunii S, Oguro I, Komatsubara T and Kasuya T 1984 *J. Phys. Soc. Japan* **53** 3967
[5] Nyhus P, Cooper S L, Fisk Z and Sarrao J 1997 *Phys. Rev.* B **55** 12 488
[6] Effantin J M, Rossat-Mignot J, Burlet P, Bartolin H, Kunii S and Kasuya T 1985 *J. Magn. Magn. Mater.* **47–48** 145
[7] Morin P, Kunii S and Kasuya T 1991 *J. Magn. Magn. Mater.* **96** 145
[8] Fisk Z, Taylor R H and Coles B R 1971 *J. Phys. C: Solid State Phys.* **4** L292
[9] Galéra R M, Osterman D P, Axe J D, Kunii S and Kasuya T 1988 *J. Appl. Phys.* **63** 3580
[10] Galéra R M, Morin P, Kunii S and Kasuya T 1992 *J. Magn. Magn. Mater.* **104–107** 1336
[11] Kunii S 1988 *J. Phys. Soc. Japan* **57** 361
[12] Segawa K, Tomita A, Iwashita K, Kasaya M, Suzuki T and Kunii S 1992 *J. Magn. Magn. Mater.* **104–107** 1233
[13] Nakamura S, Goto T, Kunii S, Iwashita K and Tamaki A 1994 *J. Phys. Soc. Japan* **63** 623
[14] Takahashi K, Nojiri H, Ohoyama K, Ohashi M, Yamaguchi Y, Motokawa M and Kunii S 1998 *J. Magn. Magn. Mater.* **177–181** 1097
[15] Morin P and Schmitt D 1990 *Handbook on Ferromagnetic Materials* vol 5, ed E P Wohlfarth and K H J Buschow (Amsterdam: North-Holland) pp 1–132
[16] Giraud M and Morin P 1986 *J. Magn. Magn. Mater.* **58** 135
[17] Aléonard R and Morin P 1985 *J. Magn. Magn. Mater.* **50** 128
[18] Aléonard R, Morin P and Rouchy J 1984 *J. Magn. Magn. Mater.* **46** 233
[19] Morin P and de Combarieu A 1975 *Solid State Commun.* **17** 975
[20] Amara M and Morin P 1995 *Physica* B **205** 379
Amara M, Morin P and Burlet P 1995 *Physica* B **210** 157
Amara M and Morin P 1996 *Physica* B **222** 61
[21] Morin P, Rouchy J and Schmitt D 1978 *Phys. Rev.* B **17** 3684
[22] Morin P, Schmitt D and du Trémolet de Lacheisserie E 1982 *J. Magn. Magn. Mater.* **30** 257
[23] Morin P, Giraud M, Burlet P and Czopnik A 1987 *J. Magn. Magn. Mater.* **68** 107
[24] Gignoux D, Schmitt D, Voiron J, Zhang F Y, Bauer E and Schaudy G 1993 *J. Alloys Compounds* **191** 139
[25] Galéra R M, Amara M, Morin P and Burlet P 1998 *J. Phys.: Condens. Matter* **10** 3883
[26] Zirngiebl E, Hillebrands B, Blumenröder S, Güntherodt G, Loewenhaupt M, Carpenter J, Winzer K and Fisk Z 1984 *Phys. Rev.* B **30** 4052
[27] Loewenhaupt M and Prager M 1986 *Z. Phys.* B **62** 195
[28] Lea K R, Leask M J M and Wolf W P 1962 *J. Phys. Chem. Solids* **23** 1381
[29] Kunii S, Iwashita K, Matsumura T and Segawa K 1993 *Physica* B **186–188** 646